applied sciences

MDPI

Article

Out-of-Plane Stability of Circular Steel Tubular Vierendeel Truss Arches Incorporating Torsional Effects of Chords

Qunfeng Liu [1,*], Yun Feng [1], Chang Wang [1], Xing Wu [2] and Xiang Ren [1]

[1] School of Architecture and Civil Engineering, Xi'an University of Science and Technology, Xi'an 710054, China
[2] CCCC First Highway Consultants Co., Ltd., Xi'an 710068, China
* Correspondence: qliu@xust.edu.cn

Abstract: Torsional stiffnesses of chords contribute considerably to the sectional torsional stiffness of steel tubular Vierendeel truss arches and hence determine their out-of-plane buckling. To obtain a more accurate stability design for the Vierendeel truss arches, torsional effects of chords on their out-of-plane stability and failure mechanisms were investigated theoretically and numerically. This paper firstly derives the theoretical formulas of the sectional torsional stiffness and the out-of-plane elastic buckling loads for the pin-ended circular steel tubular Vierendeel truss arches. It is found that incorporating the torsional stiffness of chords can remarkably enhance the sectional torsional stiffness of the Vierendeel truss arches and their out-of-plane elastic buckling loads by ~41%. Then, the out-of-plane elastic buckling loads are calculated for the pin-ended arches by the equilibrium theorem and for the fix-ended arches by the numerical fitting. In both cases, the sectional torsional stiffness and elastic buckling loads are closely dependent on the transverse-to-chord member stiffness ratio (i_t/i_c). Furthermore, the out-of-plane inelastic buckling behaviors are investigated numerically in the end-fixed Vierendeel truss arches with large i_t/i_c, where the ultimate bearing load in full-span radially uniform manner can be significantly enhanced by ~43% by incorporating the torsional stiffness of chords. The calculated reduction factors confirm the design curve b from GB50017-2017 or Eurocode 3 and can provide a conservative design for the out-of-plane stability of the circular steel tubular Vierendeel truss arches.

Keywords: elastic buckling load; inelastic buckling; out-of-plane stability; torsional stiffness; Vierendeel truss arches

Citation: Liu, Q.; Feng, Y.; Wang, C.; Wu, X.; Ren, X. Out-of-Plane Stability of Circular Steel Tubular Vierendeel Truss Arches Incorporating Torsional Effects of Chords. *Appl. Sci.* **2023**, *13*, 5082. https://doi.org/10.3390/app13085082

Academic Editor: Alberto Campagnolo

Received: 12 March 2023
Revised: 16 April 2023
Accepted: 17 April 2023
Published: 19 April 2023

1. Introduction

Vierendeel truss arches are preferred for obtaining larger spacing, concise appearance, and functional flexibility in long-span spatial structures such as bridges, stadiums, and railway stations [1]. In the classical Pratt or Warren truss arches, chord members bear compression and bending actions transferred from the external loadings, and diagonal members bear most of the shears along the centroid axis of the arches. By contrast, in the Vierendeel truss arches [2,3], no diagonal members exist and only the chords can be used to resist the sectional shears. The weak shear resistance may determine the strength design and thereby the in-plane and out-of-plane stability design of the Vierendeel truss arches in practical applications.

With adequate lateral bracings, arches under compression and bending tend to deform and fail in the in-plane modes. Pi and his coauthors revealed the elastic and inelastic in-plane buckling behaviors for the pin-ended and end-fixed arches and proposed the strength design equation for the I-section steel arches subjected to combined compressive and bending actions [4–7]. Guo et al. investigated the in-plane failure mechanism of the pin-ended circular steel arches with welded hollow sections numerically and proposed the strength design formula accounting for web local buckling [8]. It was also reported that the sectional shear stiffness played an important role in determining the elastic-plastic stability

in circular arches [9]. Further, Guo et al. derived the in-plane elastic buckling loads with the consideration of the effect of shear deformation and proposed an interaction design equation for the circular steel tubular Vierendeel planar truss arche [10]. Moreover, the shear effects of chords were taken into accounted to obtain the in-plane elastic buckling loads for the pin-ended circular Vierendeel-like steel planar arches, i.e., the plate-tube-connected arches and the web-opened steel arches [11–13]. It can be concluded that considering the sectional shear deformation may produce a much lower in-plane buckling load in truss arches than that calculated by the Timoshenko equation [14].

To meet functional or architectural needs, some arches are designed with sparse lateral bracings [15,16]. With inadequate lateral supports, the arches may deform in the flexural–torsional modes and fail in the out-of-plane before their in-plane failures if there exist considerable initial out-of-plane geometric imperfections [17,18]. The timeline for some researches on the out-of-plane stability of circular steel arches is shown in Figure 1. Timoshenko and Gere [19] first derived the out-of-plane elastic buckling load for arches under compression-only or bending-only actions based on the equilibrium theorem. Using the energy-based approach, Papangelis and Trahair derived the elastic flexural–torsional buckling loads for the pin-ended arches [20–22], and Pi et al. derived the elastic flexural–torsional buckling resistance of the laterally end-fixed circular arches [23–25]. However, these analytical results were derived from the close-section arches bearing uniform compression or uniform bending. Furthermore, Pi and Bradford studied the inelastic flexural–torsional buckling and proposed a design equation for end-fixed steel I-section arches using the finite element method [26]. These out-of-plane buckling behaviors were consistent with the experimental results by Guo et al. [27].

Moreover, for the circular steel tubular truss arches, out-of-plane buckling behaviors were reported to be affected by their end restraints and sectional stiffnesses. The effect of the end restraints was investigated by Dou and Pi on the out-of-plane buckling resistance numerically [28], and the shear stiffness of the chords of the pin-ended circular arches was considered by Dou et al. to derive the out-of-plane buckling loads analytically [29]. Few studies have been reported on the contribution of the torsional effects of chords to the out-of-plane elastic buckling loads. It is noted that, in Pratt and Warren truss arches, the sectional torsional stiffness is mostly contributed by the shear stiffness of their diagonal tubes and chords, and the contribution from the torsional stiffness of chords can be ignored [30]. However, in the sectional torsional stiffness of the Vierendeel truss arches, the contribution from the torsional stiffness of chords becomes remarkable and can be comparable with that from the shear stiffness of chords.

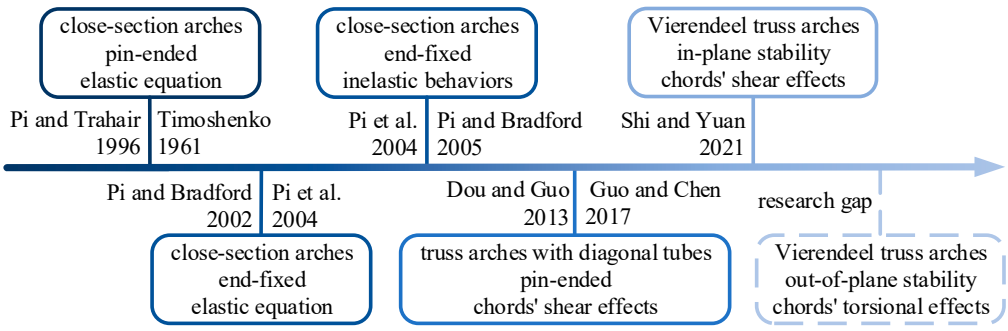

Figure 1. Timeline for researches on the out-of-plane stability of circular steel arches [4,6,7,10,14,19,23–26,29].

To date, the torsional effects of the chords on the out-of-plane inelastic failure mechanism of the Vierendeel truss arches are still unclear. There are scarce design recommendations on the out-of-plane stability of Vierendeel arches in the current design codes or the literatures. Taking the torsional deformation of chords into account might reduce the local buckling loads of truss arches slightly, whereas incorporating the torsional stiffness of chords will increase the sectional torsional stiffness/resistance considerably. Thus, the

torsional effects of chords can be deliberately ignored for a conservative strength design in the truss arches with diagonal tubes. However, in the Vierendeel truss arches where the sectional torsional stiffness is small, the torsional stiffness of chords should be taken into account for achieving better architectural aesthetics and economic demand.

In this study, the out-of-plane global elastic buckling loads were derived for the pin-ended and end-fixed circular steel tubular Vierendeel truss arches on different sectional stiffness assumptions. The main finding is that incorporating the torsional effects of chords can remarkably strengthen the global out-of-plane stability of the circular steel tubular Vierendeel truss arches. Further, the out-of-plane elastic-plastic failure mechanisms were investigated for the end-fixed arches under different loading cases. The paper is organized as follows: Section 2 introduces the finite element models of the typical Vierendeel truss arches used for static analyses; Section 3 derives the sectional stiffnesses analytically in the Vierendeel truss arches; Section 4 calculates the out-of-plane elastic buckling loads for the pin-ended and end-fixed circular tubular Vierendeel truss arches based on the derived and numerically fitted equations, respectively; Section 5 presents the out-of-plane inelastic buckling behaviors of the Vierendeel truss arches under different loading cases; some conclusions are drawn in Section 6.

2. Finite Element Models

Figure 2 shows the schematic model of a typical circular steel tubular Vierendeel truss arch studied in this work. The truss arch is constructed by four circular steel tubular chords arranged at the four corners of the rectangular cross-section. All chords are segmented by a set of rectangular diaphragms made of four connected transverse tubes that are distributed normal to the arch's sectional centroid axis with a constant interval. In each segment, no diagonal tubes are included.

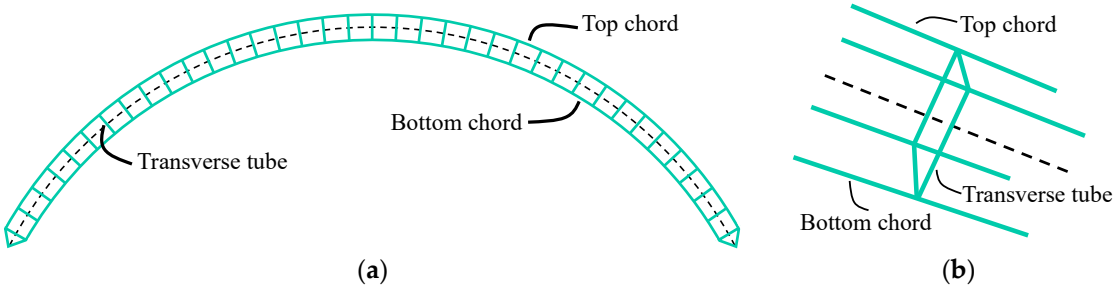

Figure 2. Schematic model of a typical circular steel tubular Vierendeel truss arch with rectangular section. (**a**) Elevation. (**b**) Diaphragm.

Figure 3 presents the geometric dimensions of the global and sectional models for a typical circular steel tubular Vierendeel truss arch. L is the arch span; f is the rise of the arch; R is the curvature radius of the cross-sectional centroid arch axis; Θ is the included angle; S (=2ΘR) is the total developed length of the arch; B and H are the width and height of the rectangular section, respectively; L_c is the segmental length between the neighboring transverse diaphragms; D_c and t_c are the outer diameter and thickness of the chords, respectively; D_t and t_t are the outer diameter and thickness of the transverse tubes, respectively.

In this study, the stability analyses of the steel tubular truss arches were performed by using the finite element (FE) software ABAQUS [31]. To consider the effect of the shear deformation on the stability of the Vierendeel truss arches, the Timoshenko beam element B31 was used to model the chord tubes and transverse tubes. All structural members in each model are meshed at a constant mesh size. We calculated the computational error for each model at different mesh sizes from 10 mm to 150 mm and found that the computational errors for models with mesh size less than 150 mm could be negligible. Thus, in this study, all models are meshed at the size of 100 mm for saving computational cost. A typical arch model with a span of 50 m and a segmental length of 1 m has 2834 nodes and 2984 meshes

in total. Two types of arches are considered with different boundary constraints: the pinned and fixe ends. In the end-fixed arch models, all translations and rotations along the x-, y-, and z-directions are fixed, while in the pin-ended arches, the translations in the y- and z-directions and the rotation along the z-direction are fixed at both ends. With these boundary constraints, circular arches are likely to bear the combined compressive and bending actions. For simplification, the translation in the y-direction of one end is usually set free to ensure the arch's cross-section under a uniform compression [32], as shown in Figure 3a. Thus, the elastic buckling loads for the pin-ended arches can be derived analytically.

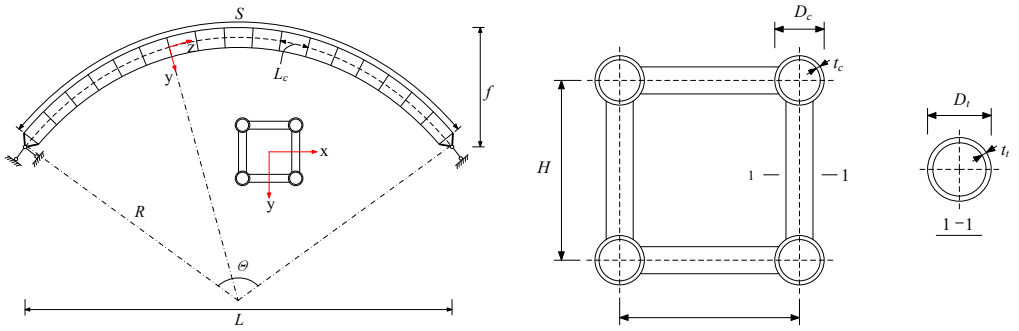

Figure 3. Geometric dimensions of a typical Vierendeel truss arch and its cross-section. (**a**) Global dimensions. (**b**) Cross-sectional dimensions.

Bilinear constitutive models were adopted for all steel tubular members. Specifically, the yielding stress for the chord tubes is 235 MPa (f_{yc}) and that for the transverse tubes is 345 MPa (f_{yt}). For all steel tubular members, the initial elastic modulus (E) is 2.06×10^5 MPa, and the Poisson's ratio (ν) is 0.3. The out-of-plane global initial geometric imperfection (with the maximum amplitude of S/500) was introduced to all FE models studied in this work, and the influence of the welding residual stress was neglected. Moreover, three typical loading cases were considered herein such as the full-span radially uniform load (FSRUL) q_r, the full-span uniformly vertical load (FSUVL) q_f, and the half-span uniformly vertical load (HSUVL) q_h, as shown in Figure 4.

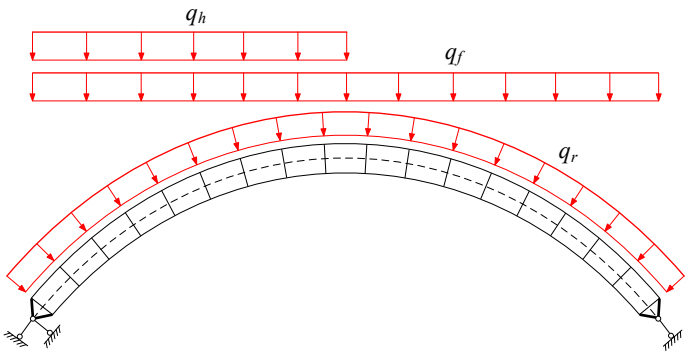

Figure 4. Different loading cases considered in this work.

3. Sectional Stiffnesses in Vierendeel Truss Arches

Without adequate bracings, the Vierendeel truss arches are likely to buckle in the out-of-plane flexural–torsional mode under compressive and bending actions. The out-of-plane stability of the truss arches is usually determined by the sectional bending stiffness, sectional shear stiffness, and sectional torsional stiffness.

3.1. Sectional Bending Stiffness and Sectional Shear Stiffness

In the circular Vierendeel truss arches, the chords may carry the axial compression, bending, and shear induced by the external loading, while the transverse tubes can only carry bending transferred from chords. Thus, the sectional bending stiffness of the chords in a truss arch is crucial for elastic stability. The out-of-plane sectional bending stiffness (EI_y) of a truss arch can be expressed as [29]:

$$EI_y = EA_cB^2 + 4EI_c \tag{1}$$

where EI_c is the bending stiffness of each chord with the identical cross-sectional area A_c.

The effect of the shear deformation of chords was reported to be very important in truss arches, and the out-of-plane shear stiffness was derived for the steel tubular truss arches with rectangular sections [29]. Without the diagonal tubes, shears acting on the cross-section of the Vierendeel truss arch can only be undertaken by chords. The sectional shear stiffness of the Vierendeel truss arches can be calculated by the equation derived by Timoshenko and Gere [19] for the battened lattice column. For a typical Vierendeel truss segment under a pure shear V, the moments carried by the chords and transverse tubes are shown in Figure 5.

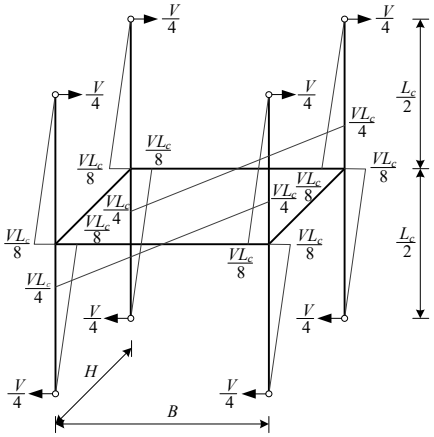

Figure 5. Moment diagram of a typical Vierendeel truss segment under the pure shear V.

The shear deformation δ of the entire cross-section comprises the segmental deformations induced by the bending moments of chords δ_1, the bending of the transverse tubes δ_2, and the shear deformation of the transverse tubes δ_3. Thus, the sectional shear deformation δ can be calculated according to the following formula:

$$\delta = \delta_1 + \delta_2 + \delta_3 = \frac{VL_c^3}{48EI_c} + \frac{VL_c^2B}{24EI_t} + \frac{nVL_c^2}{2BA_tG} \tag{2}$$

Accordingly, the sectional shear stiffness (K_V) of the typical truss segment can be calculated as:

$$K_V = \frac{1}{\frac{L_c^2}{48EI_c} + \frac{L_cB}{24EI_t} + \frac{nL_c}{2BA_tG}} \tag{3}$$

where EI_c is the sectional bending stiffness of each chord; EI_t is the sectional bending stiffness of each transverse tube. G (=$E/2$ (1 + ν)) is the shear modulus. n is the non-uniform distribution coefficient of shear stress in the cross-section of the transverse tubes. For the transverse tube with an annular section, n is 2.0 and the sectional area is A_t [19].

3.2. Sectional Torsional Stiffness

To calculate the sectional torsional stiffness, Guo et al. assumed the web-open truss arch to be an equivalent thin-walled box arch with a hollow rectangular section composed

of four thin plates [33]. With the equivalent box cross-section, the torsional stiffness of a typical Vierendeel truss arch can be expressed as:

$$\begin{cases} GJ = G\dfrac{4A_0^2}{\sum\limits_{i=1}^{4}\dfrac{l_i}{t_{ri}}} \\ t_{ri} = \dfrac{E}{G} \times \dfrac{1}{\dfrac{L_c^2 l_i}{24I_c} + \dfrac{L_c l_i^2}{12I_t}} \end{cases} \tag{4}$$

where l_i is the i-th side length of the rectangular section, t_i is the thickness of the i-th box side plate, A_0 is the area of the rectangular section.

Since the spans (L) of the considered truss arches (over 20 m) are much larger than the sectional side length (B or H), the influence of the arch curvature on the sectional torsional stiffness can be ignored for simplification. An equivalent straight truss model is thus built with a length of 100 m and a square cross-section ($H = B = 1.0$ m). To verify the sectional torsional stiffness, static analyses via the FE program ABAQUS were performed on the equivalent straight truss. In the long-span truss models, boundary conditions were confirmed to have little influence on the sectional torsional stiffness. Herein, the bottom end of each chord is pinned to the ground, and the torsion M_z is applied on the top free section, as shown in Figure 6a.

Under the torsional moment M_z, the sectional twist around the centroid axis z is resisted by the shears of chords along the transverse tubes, as shown in Figure 6. Thus, the torsional equilibrium of a typical truss segment can be calculated as:

$$\begin{cases} \vec{V_1} + \vec{V_2} + \vec{V_3} + \vec{V_4} = 0 \\ \sum\limits_{i=1}^{4} V_i r_i = M_z \end{cases} \tag{5}$$

where r_i (i = 1~4) is the distance from the torsion centroid (O) to the i-th side of the rectangular section, and V_i is the shear along the i-th transverse tube. In each segment, the shear stiffness of each chord can be expressed as:

$$K_{V_i} = \frac{V_i}{r_i \beta / L_c} \tag{6}$$

where β is the sectional rotation angle of a Vierendeel truss segment under the external torsion moment M_z. Accordingly, the sectional torsional stiffness can be calculated as:

$$GJ = \frac{M_z}{\beta / L_c} = \sum_{i=1}^{4} K_{V_i} r_i^2 \tag{7}$$

Further, the sectional torsional stiffness can be written as:

$$GJ = \frac{H^2}{\dfrac{L_c^2}{12EI_c} + \dfrac{L_c B}{6EI_t} + \dfrac{2nL_c}{BA_t G}} + \frac{B^2}{\dfrac{L_c^2}{12EI_c} + \dfrac{L_c H}{6EI_t} + \dfrac{2nL_c}{HA_t G}} \tag{8}$$

When the torsional stiffness of chords is considered, the sectional twist will be resisted by both the shear and torsion of each chord, as shown in Figure 7. Thus, the torsional equilibrium of a typical truss segment can be calculated as:

$$\begin{cases} \vec{V_1} + \vec{V_2} + \vec{V_3} + \vec{V_4} = 0 \\ \sum\limits_{i=1}^{4} (V_i r_i + M_i) = M_z \end{cases} \tag{9}$$

where M_i (i = 1~4) is the torsion moment carried out by the i-th chord. Under the sectional torsion M_z, the torsional stiffness contributed by each chord (GI_{pci}) can be expressed as:

$$GI_{pci} = \frac{M_i}{\beta / L_c} \tag{10}$$

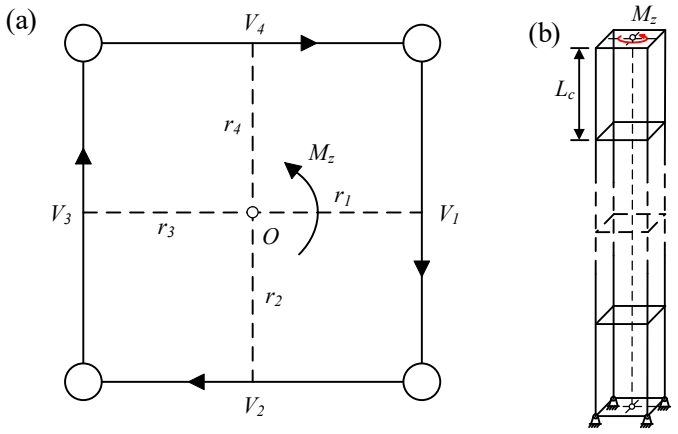

Figure 6. Torsion diagram (**a**) of a typical cross-section in the equivalent straight truss (**b**) considering the shear deformation of chords.

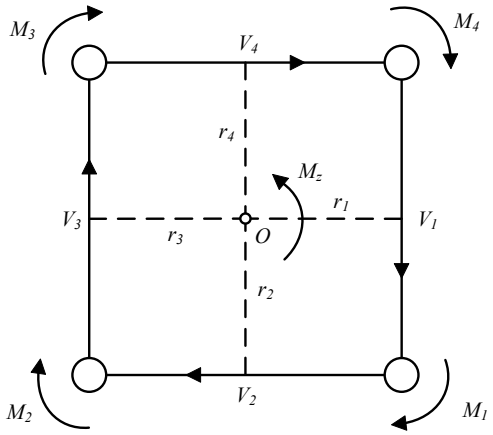

Figure 7. Torsion diagram of a typical cross-section in the equivalent straight truss considering the torsional stiffness of chords.

Thereby, the sectional torsional stiffness of the segment can be derived by:

$$GJ = \frac{M_z}{\beta / L_c} = \sum_{i=1}^{4} \left(K_{V_i} r_i^2 + GI_{pci} \right) \tag{11}$$

Substituting Equation (3) into Equation (11) yields the sectional torsional stiffness of the segment including the torsional stiffness of each chord. Thus, the sectional torsional stiffness can be rewritten as:

$$GJ = \frac{H^2}{\frac{L_c^2}{12EI_c} + \frac{L_c B}{6EI_t} + \frac{2nL_c}{BA_t G}} + \frac{B^2}{\frac{L_c^2}{12EI_c} + \frac{L_c H}{6EI_t} + \frac{2nL_c}{HA_t G}} + 4GI_{pc} \tag{12}$$

It can be noted that the sectional torsional stiffness of the straight truss model is primarily determined by the shear stiffness (K_{Vi}) and torsional stiffness (GI_{pci}) of individual chords. Further, the shear and torsional stiffnesses of chords are influenced by their constraints exerted by the neighboring transverse tubes. Thus, the torsional effects of

chords on the sectional torsional stiffness should be investigated in trusses with different transverse tubes and chords. Here, the segmental length (L_c), the external diameter (D_c), and wall thickness (t_c) of the chord tubes are set to be constant at 1000 mm, 121 mm, and 10 mm, respectively; the external diameters (D_t) ranging from 20 mm to 200 mm with a constant wall thickness (t_t) of 10 mm, are set for the transverse tubes.

Figure 8a shows the sectional torsional stiffnesses (GJ) of a series of models with different segmental lengths. In this case, the member stiffnesses of chords decrease with the increase in the segment length (L_c) from 1.0 m to 4.5 m in the arches with the constant transverse tubes with D_t of 121 mm and t_t of 10 mm. It is observed that, for results calculated by either equation or the FE simulation, the sectional torsional stiffness decreases with the increase in the L_c, and the curve of the torsional stiffness versus L_c flattens as the L_c increases beyond 4.0 m. Figure 8b shows the sectional torsional stiffnesses of a series of models with different transverse-to-chord member stiffness ratios (i_t/i_c) at a constant L_c of 1.0 m. It is observed that the sectional torsional stiffness increases with the increase in i_t/i_c and approaches a plateau when i_t/i_c increases beyond a threshold of ~6, confirming that the sectional torsional stiffness of the Vierendeel truss arch is closely dependent on i_t/i_c [29]. Further, it can be concluded that, for the arches with i_t/i_c ranging from 0.1 to 9.0 and L_c from 1.0m to 4.5 m, the torsional stiffnesses obtained by Equation (12) agree well with that from the FE simulations, and both are much larger than that obtained by Equations (4) and (8). Some key equations and their assumptions are liste in Table A1 (Appendix A). The remarkable discrepancy indicates that incorporating the torsional stiffness of an individual chord can significantly enhance the sectional torsional stiffness of the Vierendeel trusses with any i_t/i_c considered here.

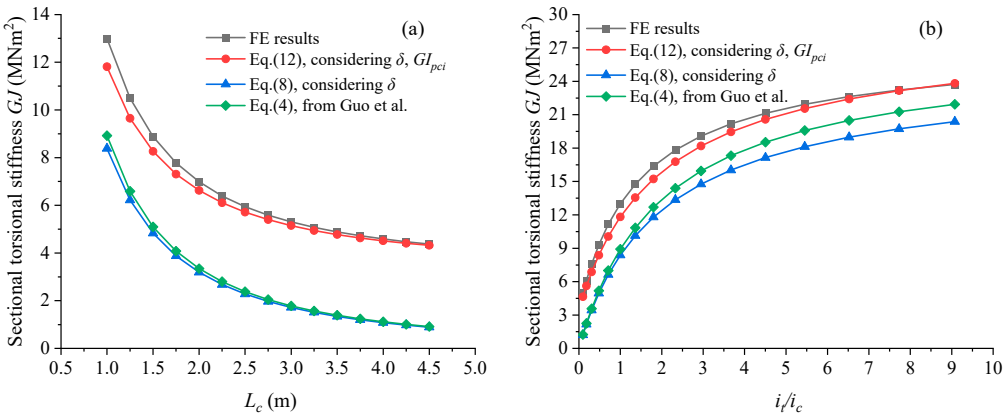

Figure 8. Sectional torsional stiffness and as a function of (**a**) segment length or (**b**) i_t/i_c for the equivalent straight trusses obtained from FE results and derived equations [33].

4. Out-of-Plane Elastic Buckling Load of Vierendeel Truss Arches

For the pin-ended truss arches with diagonal tubes, Dou et al. have derived an out-of-plane buckling load incorporating the shear effect of chords using the static equilibrium approach [29]. Under the full-span uniform radial load (FSURL), the out-of-plane critical buckling load (q_{cr}) for the truss arches can be expressed as:

$$q_{cr} = \frac{q_{cr0}}{1 + q_{cr0}R/K_V} \tag{13}$$

where K_V is the sectional shear stiffness of the truss arch, q_{cr0} is the out-of-plane critical buckling load of the truss arch without considering the shear deformation of chords.

According to Kirchhoff's equation [19], the elastic out-of-plane buckling load of the pin-ended circular solid-web arch under the FSURL can be derived as:

$$q_{cr0} = \frac{P_y\left[1-(\Theta/\pi)^2\right]^2}{R\left[1+(EI_y/GJ)(\Theta/\pi)^2\right]} \tag{14}$$

where P_y is the equivalent axial buckling compression obtained in the first flexural buckling mode of the truss arch around the *o*-*y* axis. The arch has a developed length of S, an in-plane radius R, and a constant cross-section. For large-span arches, the P_y can be approximately calculated as:

$$P_y = \frac{\pi^2 EI_y}{S^2} \tag{15}$$

Figure 9 shows the buckling loads obtained by the proposed Equations (13) and (14), and the FE simulations for the circular steel tubular Vierendeel truss arches at different spans (L), segmental lengths (L_c), sectional side lengths (B), and transverse-to-chord member stiffness ratios (i_t/i_c). The dimensions (L, L_c, and B) of the typical Vierendeel truss arch are initially set to be 50 m, 1.0 m, and 1.0 m, respectively. The influence of each dimension on the buckling load can be studied independently by fixing two other dimensions at their initial values. For all cases, the rise-to-span ratio (f/L) is fixed at 0.2; the external diameter (D_c) and wall thickness (t_c) of each chord are kept at 152 mm and 8 mm, respectively.

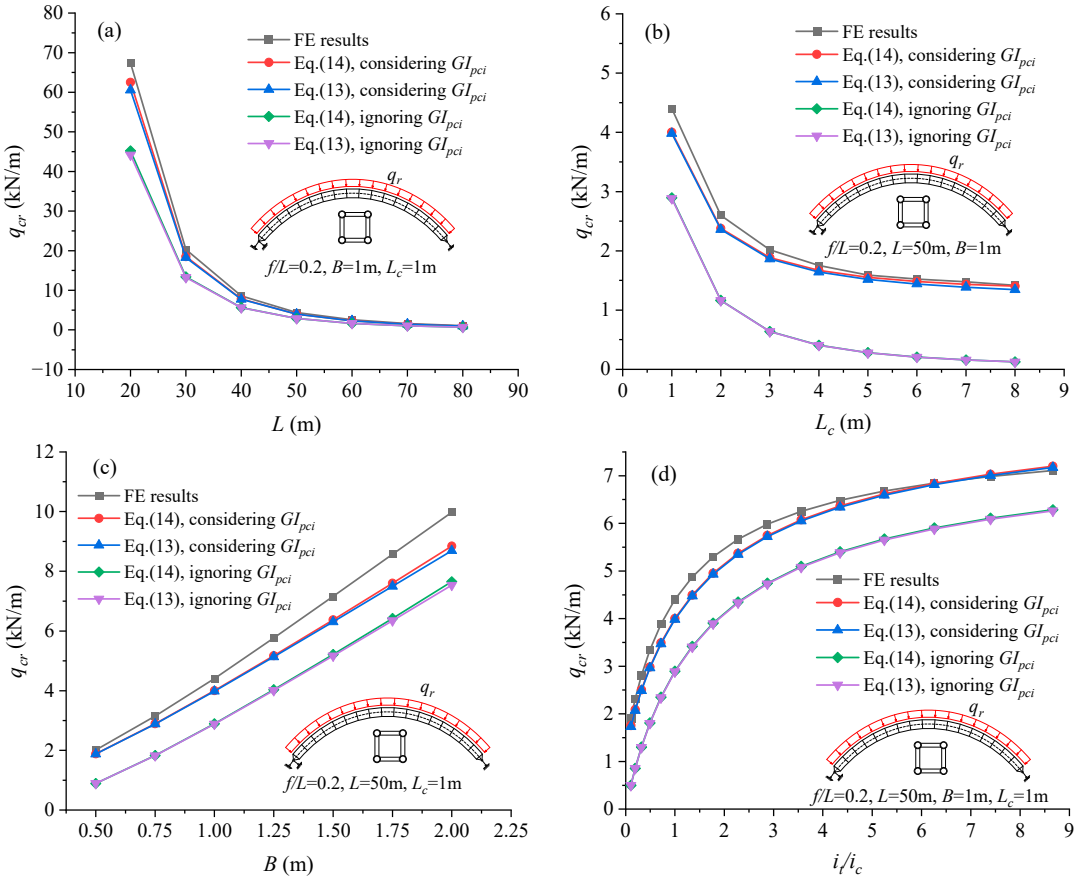

Figure 9. Comparison of buckling loads between FE and theoretical results for the pin-ended Vierendeel truss arches with varying (**a**) spans, (**b**) segmental lengths, (**c**) sectional side lengths, and (**d**) transverse-to-chord member stiffness ratios.

As observed in Figure 9a–d, the buckling loads in the FSURL manner (q_{cr}) decrease with the increase in L (or L_c) but increase with the increase in i_t/i_c (or B). For all cases considered in this study, the buckling loads calculated from Equations (13) and (14), either

incorporating the torsional effects of chords or not, agree well with each other. This indicates that both the Kirchhoff equation and the equation derived by Dou et al. [29] can predict nearly identical out-of-plane buckling loads for large-span truss arches. It is also noted that the buckling load for cases incorporating the torsional effects of chords is generally larger than that for cases ignoring the torsional effects of chords, as shown in Table 1. This indicates that the torsional effects play a significant role in determining the buckling loads (q_{cr}). However, for the arches with spans larger than 70 m, as shown in Figure 9a, the discrepancy due to the torsional effects becomes negligible.

Table 1. Increment of the average buckling load over the considered dimensions for the pin-ended Vierendeel truss arches considering GI_{pci} with respect to that ignoring GI_{pci}.

Dimension	L (=50 m)	L_c	B	i_t/i_c
Increment of average q_{cr} by Equation (13)	37.93%	429.39%	52.15%	41.45%
Increment of average q_{cr0} by Equation (14)	38.30%	442.88%	52.61%	41.67%

Figure 9b,c show the numerically and theoretically obtained buckling loads of the truss arches as a function of the segmental length and the sectional side length, respectively. Generally, the buckling loads for all cases (L = 50 m) decrease with the segmental length (L_c) and increase with the sectional side length (B). It is also observed that the buckling loads calculated by Equations (13) and (14), incorporating the torsional stiffness of chords or not, are consistent with each other. The calculated loads incorporating the torsional effects are remarkably larger than that, if we ignore the torsional effects but slightly smaller than the FE results. Moreover, the deviation between the FE results and the theoretical results incorporating the torsional effects decrease with L_c and increase with B.

Figure 9d presents the relationship between q_{cr} and the transverse-to-chord member stiffness ratio (i_t/i_c), which represents the combined influence of L_c and B. Generally, q_{cr} increases rapidly as i_t/i_c increases from 0.1 to 3.0 and then increases gradually approaching a plateau as i_t/i_c increases beyond 6.0. It is also noted that the q_{cr} calculated from Equations (13) and (14) considering the torsional effects are consistent with the FE results and much larger than that from these equations if we ignore the torsional effects. This trend is similar to the relationship between the sectional torsional stiffness and member stiffness ratio (i_t/i_c), indicating that i_t/i_c may play a critical role in determining the out-of-plane buckling loads of the Vierendeel truss arches.

In practice, the ends of large-span truss arches are usually fixed for better flexural and torsional resistance. However, the buckling load formulas for the end-fixed arches are too difficult to derive analytically. Here, a fitted formula is proposed based on the out-of-plan static analyses of the end-fixed truss arches conducted by the FE simulations. Based on the simulations, the buckling load formulas for the end-fixed Vierendeel truss arches can be expressed as:

$$\begin{cases} q_{cr} = \dfrac{q_{cr0}}{1 + q_{cr0}R/K_V} \\ q_{cr0} = \dfrac{4\pi^2 EI_y}{S^2 R}\left[A\left(\dfrac{\Theta}{\pi}\right)^2 + B\left(\dfrac{\Theta}{\pi}\right) + 0.85\right] \end{cases} \tag{16}$$

where

$$\begin{cases} A = 1258.18\left(\dfrac{GJ}{EI_y}\right)^2 - 90.11\left(\dfrac{GJ}{EI_y}\right) + 1.84 \\ B = -1435.94\left(\dfrac{GJ}{EI_y}\right)^2 + 97.89\left(\dfrac{GJ}{EI_y}\right) - 2.76 \end{cases} \tag{17}$$

Figure 10 shows the buckling loads of a set of Vierendeel truss arches with identical geometric dimensions: $D_c \times t_c$ = 121 mm × 10 mm, $D_t \times t_t$ = 100 mm × 10 mm, $B = H = L_c$ = 1.0 m, and L = 50 m. For the truss arches with f/L ranging from 0.1 to 0.45, the buckling loads calculated by the fitted Equation (16) agree well with the FE simulations (the maximum error is within 5%). These results are much larger than that of the pin-ended

arches calculated by Equation (13), confirming the enhanced buckling resistances in the truss arches with fixed ends.

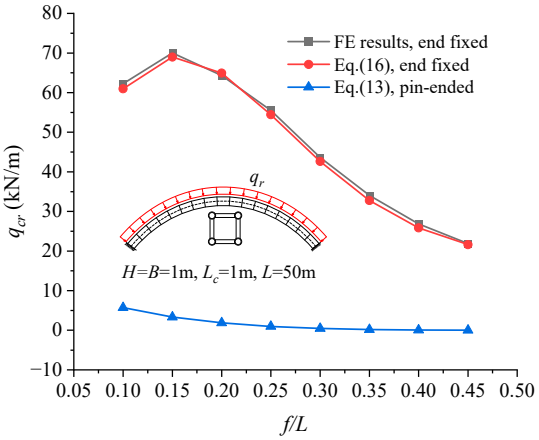

Figure 10. Comparison of buckling loads between FE and theoretical results for the end-fixed Vierendeel truss arches with different rise-to-span ratios.

Figure 11 shows the buckling loads for the end-fixed Vierendeel truss arches, with identical geometric dimensions as the corresponding the pin-ended arches shown in Figure 8. In the end-fixed arches, the changing trends of the buckling loads with L, L_c, B, and i_t/i_c are similar to that of the pin-ended arches. For all cases considered here, the buckling loads of the end-fixed arches calculated by Equation (16) agree well with the FE results and are much larger than that of the pin-ended arches. In addition, the buckling loads incorporating the torsional stiffness of chords are remarkably larger than that ignoring the torsional effects.

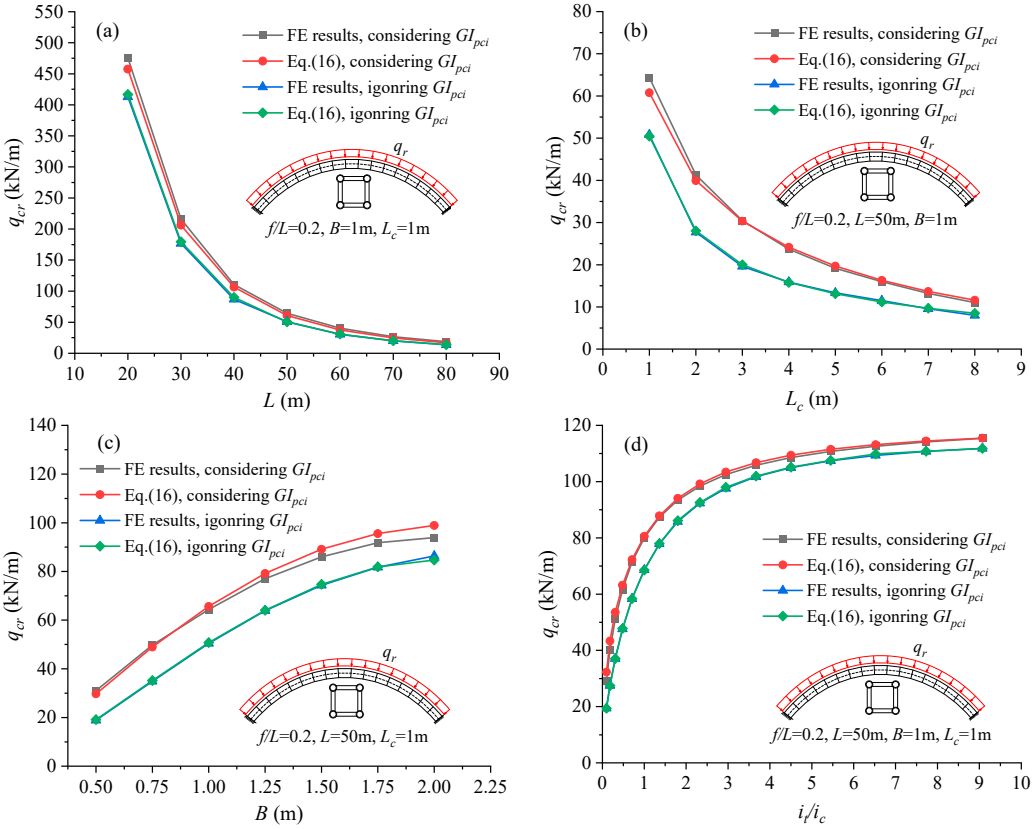

Figure 11. Comparison of buckling loads (q_{cr}) between FE and theoretical results for the end-fixed Vierendeel truss arches with varying (**a**) spans, (**b**) segmental lengths, (**c**) sectional side lengths, and (**d**) transverse-to-chord member stiffness ratios.

5. Out-of-Plane Inelastic Buckling Behaviors of Vierendeel Truss Arches

5.1. Cases under the FSURL

It has been reported that the buckling behaviors of the truss arches (locally or globally) are dependent of their loading cases [17]. Here, three typical loading cases (FSURL, FSUVL, and HSUVL) were considered to study the elastic-plastic out-of-plane buckling behaviors of the Vierendeel truss arches. Under the full-span uniform radial load (FSURL), the end-fixed circular truss arches bear large compression and small bending. To prevent the elastic local buckling before the global buckling, the Chinese Code for Design of Steel Structures (GB50017-2017) recommended that the slenderness ratio of a single chord λ_c should meet the following requirements [34]:

$$\lambda_c < \min\{0.5\lambda_{oy}, 40\} \tag{18}$$

Here, λ_{oy} is the equivalent slenderness ratio of the truss segment, which can be expressed as:

$$\lambda_{oy} = \sqrt{\lambda_y^2 + \frac{\pi^2}{12}\lambda_c^2\left(1 + \frac{2i_c}{i_t}\right)} \tag{19}$$

where λ_y is the out-of-plane slenderness ratio of the truss segment, i_c and i_t are the member stiffnesses of chords and transverse tubes, respectively.

Given a set of the Vierendeel truss arches having f/L = 0.3, L = 50 m, $B = H = L_c$ = 1.0 m, $D_c \times t_c$ = 121 mm × 10 mm, and $D_t \times t_t$ = 200 mm × 10 mm, λ_c can thus be calculated to be 25.4, which satisfies the Equation (18), meaning that the local buckling can be prevented before the global buckling. According to the FE results, the relationship between the vault displacements (out-of-plane u and in-plane w) and the uniform radial load (q_r) can be established, as shown in Figure 12. It is seen that both vault displacements (u, w) of the arches (L = 50 m) increase with the increase in the load q_r. Under the increased q_r, the arches deform out of the arch plane due to the global out-of-plane geometric imperfection ($S/500$), leading to a second-order bending along the o-y axis, and results in the out-of-plane buckling. It is noted that the out-of-plane ultimate load (ignoring the torsional stiffness of chords) is 42.1 kN/m, shown as point A_1 in Figure 11, which is much less than that (60.2 kN/m) in cases considering the torsional effects, shown as point A in Figure 11. For comparison, the in-plane ultimate load of a typical arch (L = 50 m, f/L = 0.3) is calculated to be 97.3 kN/m by introducing a global in-plane geometric imperfection ($S/500$) alternatively. Figure 13 presents the overall stress distribution of the typical arch under the ultimate FSURL (corresponding to point A). Under the combined actions of compression and bending, the initial yielding starts from the four symmetric spots: the right chords at both arch feet and the top-right chords at the 3/8 and 5/8 of the span. After that, the arch fails in a symmetric inelastic global buckling mode, accompanied by the decrease in q_r and the further increase in u.

According to Pi et al. [35], the normalized slenderness of an arch can be defined as:

$$\lambda_n = \sqrt{\frac{N_y}{N_{cr}}} = \sqrt{\frac{4A_c f_{yc}}{q_{cr}R}} \tag{20}$$

where N_y and N_{cr} are the yielding and critical compressions on the cross-section of the truss arch, respectively; q_{cr} is the out-of-plane elastic critical FSURL of the truss arch and can be calculated by Equation (16). Thus, the reduction factor (φ) for the out-of-plane ultimate strength relative to the yielding strength of the Vierendeel truss arches can be defined as:

$$\varphi = \frac{N_u}{N_y} = \frac{q_u R}{4A_c f_{yc}} \tag{21}$$

where N_u is the ultimate compression on the cross-section of the truss arch and q_u is the ultimate bearing load in the FSURL manner. It is acknowledged that the ultimate bearing capacity of a truss arch is closely related to its f and L [17]. Here, we performed a series of FE

static analyses on the considered Vierendeel truss arches with different spans (20 m~60 m) and rise-to-span ratios ranging from 0.1 to 0.5. Based on the FE results, the reduction factors at various λ_n are calculated and presented in Figure 14. For comparison, the compression-only column design curves *a*, *b*, *c*, and *d* from the Chinese Code for Design of Steel Structures (GB50017-2017) and Eurocode 3 [36] are also presented herein. It can be observed that the numerically obtained reduction factors are approximately located between the curve *a* and the curve *b* from both codes, except for the cases with very small f/L (0.1~0.2). This indicates that the curve *b* may provide a conservative prediction of φ for the ultimate bearing capacity of the steel tubular Vierendeel truss arches with large f/L. Thus, the reduction factor on the curve *b*, referred from either GB50017-2017 or Eurocode 3, can be used to check the design strength (N) determined by the out-of-plane stability using the design formula:

$$\frac{N}{\varphi N_y} \leq 1 \tag{22}$$

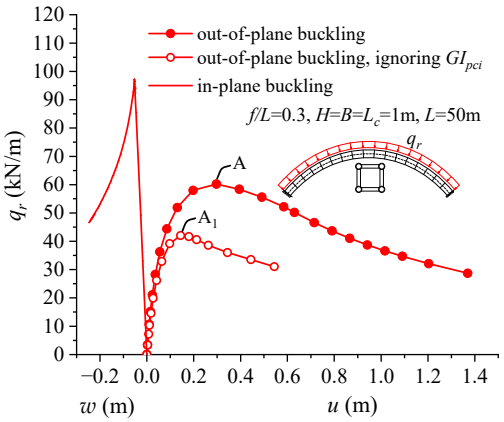

Figure 12. In-plane and out-of-plane vault displacements of a typical end-fixed Vierendeel truss arch under FSURLs.

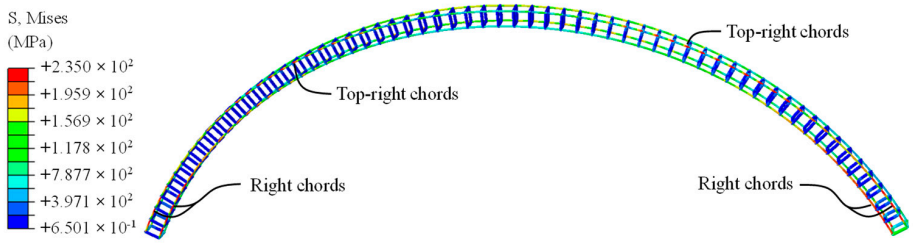

Figure 13. Stress distribution of a typical Vierendeel truss arch under the ultimate FSURL.

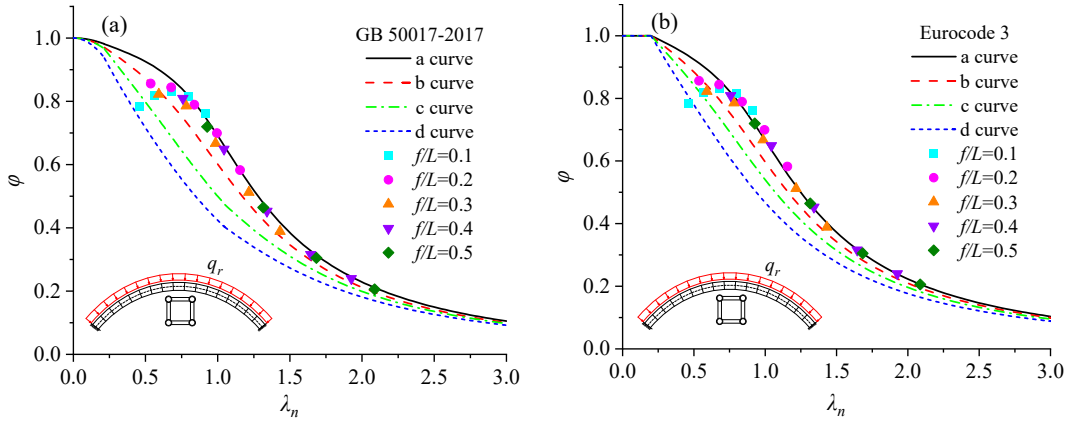

Figure 14. Design curves and numerically obtained reduction factors for the end-fixed Vierendeel truss arches under FSURLs. (**a**) result of FE and GB 50017. (**b**) result of FE and Eurocode 3.

5.2. Cases under the FSUVL

Under the full-span uniform vertical load (FSUVL), the end-fixed circular truss arches tend to be under the combined actions consisting of compression, bending, and shear. For comparison, the set of the Vierendeel truss arches under the FSUVL, with the same dimensions as the previous cases under the FSURL, was investigated based on the FE inelastic analyses. In these cases, elastic local buckling can also be prevented before global buckling with the same small λ_c. Figure 15 shows the variations of the uniform vertical load (q_f) with the vault out-of-plane displacement (u) for the arches (L = 50 m). It is seen that the load q_f for a typical arch (L = 50 m, f/L = 0.3) increases with the increase in the out-of-plane vault displacement and reaches its ultimate value for the case ignoring the torsional stiffness of chords at 26.8 kN/m, shown as point B_1, which is smaller than that (32.2 KN/m) in the case incorporating the torsional effects, shown as point B. Figure 16 presents the overall stress distribution of the typical arch under the ultimate FSUVL (corresponding to point B). It is seen that the truss arch firstly yields at both feet of chords, and then buckles under the ultimate load. This behavior confirms the findings by Guo et al. [10] that local yielding of chords will occur before global buckling in the planar Vierendeel truss arches with i_t/i_c larger than 2.25. Thereafter, with the further increase in u, the yielding spots develop from the feet to the quarters along the arch until it fails eventually.

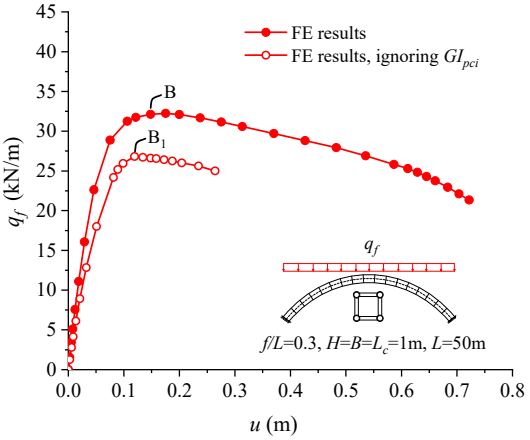

Figure 15. Out-of-plane vault displacements of the typical Vierendeel truss arch under FSUVLs.

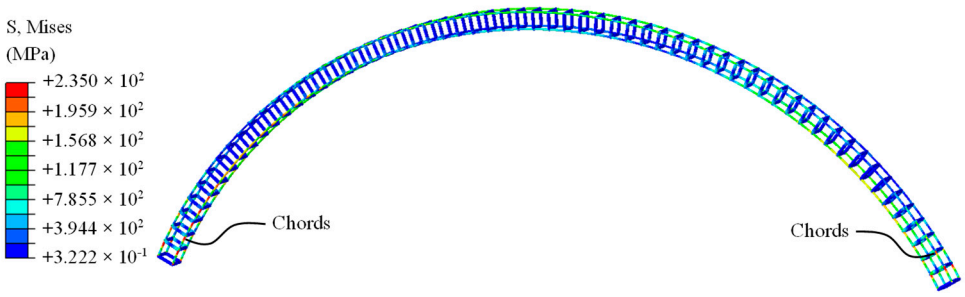

Figure 16. Stress distribution of the typical Vierendeel truss arch under the ultimate FSUVL.

Under the FSUVL, the end-fixed truss arches usually bear compression and bending simultaneously. Thus, an interaction strength design equation can be deduced to check the ultimate design strength, which is expressed as [27,37,38]:

$$\frac{N^*}{\varphi N_y} + \frac{\alpha M^*}{M_y} \leq 1 \tag{23}$$

where N^* and M^* are the maximum axial compression and the maximum bending moment of the Vierendeel truss arches based on the first-order elastic analyses, respectively; N_y

and M_y are the compression and bending moment at yielding of the whole cross-section, respectively; φ is the out-of-plane reduction factor for the buckling compressions of the truss arches under the FSUVL and can be referred from the curve *b* from the GB50017-2017. Since the Vierendeel truss arches do not have diagonal tubes to resist shear, they possess small sectional shear stiffness. Thus, the second-order sectional bending moment under shear should be considered by multiplying the M^* with a moment amplification factor α that can be calculated as:

$$\alpha = \frac{1}{1 - \frac{N^*}{q_{cr}R}} \tag{24}$$

where q_{cr} is the elastic buckling load of the arches in the FSURL manner given by Equation (14). It has been verified that, when α is less than 1.4, the first-order moment amplified by α can provide a good estimation of the second-order moment [4]; when α is larger than 1.4, the modified bending moment (αM^*) should be replaced by the second-order moment obtained numerically.

Based on the FE analyses, we obtained the maximum strength pairs ($N^*/(\varphi N_y)$, $\alpha M^*/M_y$) for the Vierendeel truss arches at different spans (20 m~60 m) and rise-to-span ratios ranging from 0.1 to 0.5. Moreover, the interaction design curve obtained by Equation (23) is presented for comparison, as shown in Figure 17. It is seen that all strength capacity pairs are above the interaction design curve, indicating that the reduction factor calculated by Equation (21) can provide a conservative prediction for the out-of-plane stability design of the end-fixed Vierendeel truss arches.

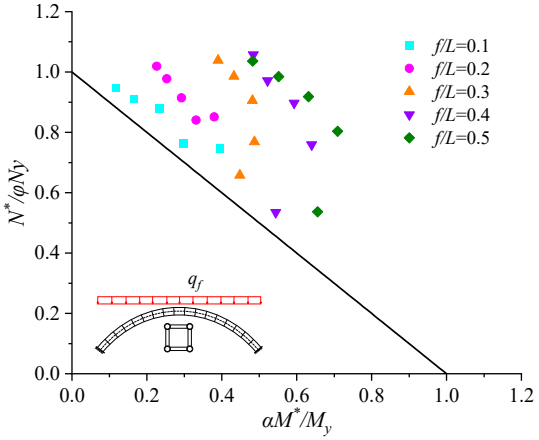

Figure 17. Comparison between the maximum strength pairs and the interaction design curve for the end-fixed Vierendeel truss arches under FSURLs.

5.3. Cases under the HSUVL

Under the half-span uniform vertical load (HSUVL), the end-fixed circular truss arches tend to be under combined actions consisting of asymmetric compression, bending, and shear. Moreover, the set of the Vierendeel truss arches under the HSUVL, with the same dimensions as previous cases, was investigated based on the FE inelastic analyses. Similarly, local buckling of chords is prevented before the global buckling by introducing a global out-of-plane geometric imperfection ($S/500$).

Figure 18 shows the variations of the half-span uniform vertical load (q_h) with the numerically obtained out-of-plane vault displacement (u) for the arches (L = 50 m). It is seen that q_h for a typical arch (L = 50 m, f/L = 0.3) increases with the increase in the out-of-plane vault displacement and reaches its ultimate value for the case ignoring the torsional stiffness of chords at 30.0 kN/m, shown as point C_1, which is smaller than that (37.8 KN/m, shown as point C) in the case incorporating the torsional effects. It can be noted that, under the q_h of 24.7 kN/m (point C_0), the arch yields at the chords of the 8/8 of the span and reaches global buckling out of the arch plane under the q_h of 37.8 kN/m. Figure 19 presents the overall stress distribution of the arch under the ultimate HSUVL

(corresponding to point C). Thereafter, with the increase in u, the plastic spots develop rapidly until the eventual failure of the arch.

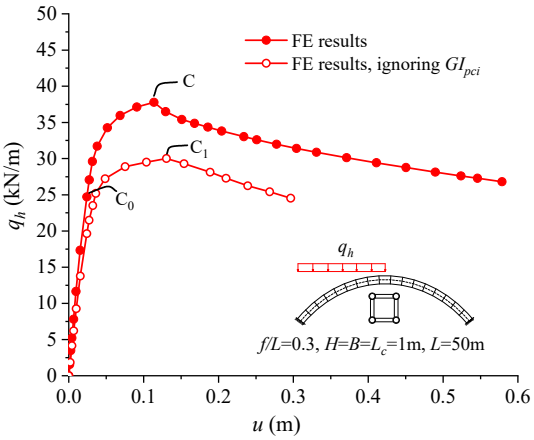

Figure 18. Out-of-plane vault displacements for the typical Vierendeel truss arch under HSUVLs.

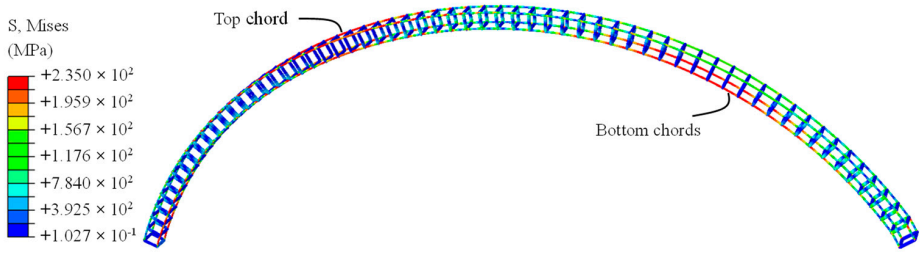

Figure 19. Stress distribution of the typical Vierendeel truss arch under the ultimate HSUVL.

Figure 19 presents the numerical obtained maximum strength capacity pairs ($N^*/(\varphi N_y)$, $\alpha M^*/M_y$) for the Vierendeel truss arches at different spans (20 m~60 m) and f/Ls ranging from 0.1 to 0.5 under the HFUVL. Compared with the interaction strength design equation, shown as the line in Figure 20, all the strength capacity pairs are observed to be well above the interaction design line, indicating that Equation (21) provides a lower bound prediction of the reduction factors for the stability design of the end-fixed Vierendeel truss arches with all considered f/Ls. Particularly, Equation (21) is much more conservative for the arches under the HFUVL. To sum up, the out-of-plane stability design of the Vierendeel truss arches under different loading cases can be conducted following the same design procedure, as shown in Figure 21.

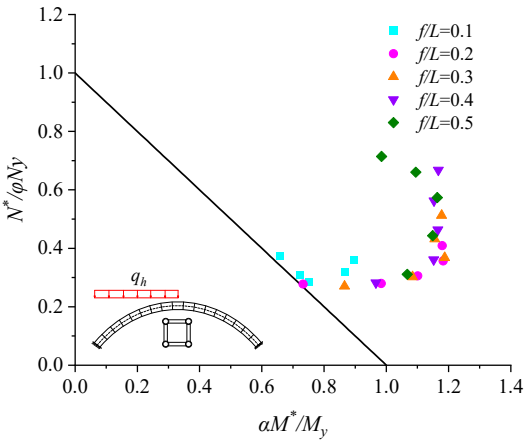

Figure 20. Comparison between the maximum strength pairs and the interaction design curve for the end-fixed Vierendeel truss arches under HSURLs.

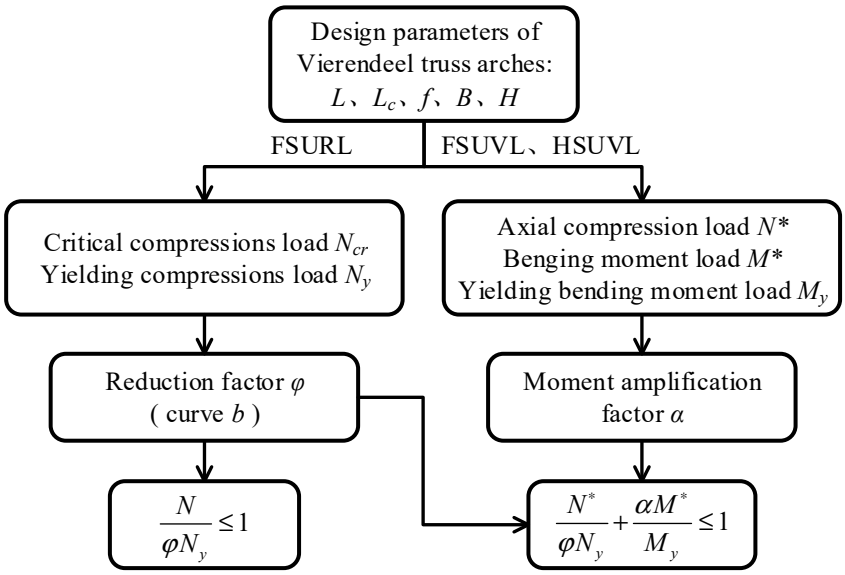

Figure 21. Out-of-plane stability design procedure of the Vierendeel truss arches.

6. Conclusions

This work reported the out-of-plane stability of the circular steel tubular Vierendeel truss arches with rectangular cross-sections under different loading cases. Considering both the shear deformation and torsion of chords, the sectional torsional stiffness of the pin-ended Vierendeel truss segment was deduced theoretically using the static equilibrium theorem. The effects of torsional stiffness of chords on the out-of-plane elastic buckling load were investigated for the circular steel tubular Vierendeel truss arches with pinned and fixed ends. Moreover, the out-of-plane elastic and inelastic buckling incorporating torsional effects were discussed for the stability design of the end-fixed Vierendeel truss arches. Some conclusions can be drawn as follows:

1. The sectional torsional stiffness of the pin-ended circular steel tubular Vierendeel truss arches decreases with the segment length but increases with the transverse-to-chord member stiffness ratio (i_t/i_c). Incorporating the torsional stiffness of individual chords can remarkably enhance the sectional torsional stiffness of the Vierendeel truss arches.
2. The out-of-plane elastic buckling loads of the circular Vierendeel truss arches, either the pin-ended cases derived by the equilibrium theorem, or the fix-ended cases derived by the numerical fitting, increase significantly when the torsional stiffness of each chord is taken into account. The dependence of the out-of-plane buckling load, similar to that of the sectional torsional stiffness on i_t/i_c, is observed in both the pin-ended and the end-fixed Vierendeel truss arches.
3. For the fixed Vierendeel truss arches with large i_t/i_c, the local yielding of chords occurs before the global buckling. Incorporating the torsional stiffness of chords will remarkably increase the ultimate buckling loads of arches under different loading cases (FSURL, FSUVL, and HSUVL). The curve *b* from the design codes (GB50017-2017 or Eurocode 3) can provide a lower bound prediction of the reduction factors for the out-of-plane stability design of the end-fixed Vierendeel truss arches.

These conclusions may provide practical guidance for the stability design of circular steel tubular Vierendeel truss arches. However, the proposed equations in this work can only provide a conservative prediction on the out-of-plane buckling loads in the Vierendeel truss arches with rectangular cross-sections at some specific dimensions. For extensive application or optimization design in practice, more research can be conducted in the near future by utilizing the optimization methods, such as the artificial neural network or the fuzzy logic algorithm [39,40], into the current design procedures to improve the adaptivity of the stability design.

Author Contributions: Q.L.: conceptualization, validation, writing—review and editing, funding acquisition; Y.F.: investigation, writing—original draft preparation, methodology; C.W.: investigation, software; X.W.: writing—review and editing, project administration; X.R.: writing—review and editing. All authors have read and agreed to the published version of the manuscript.

Funding: This research was funded by the National Natural Science Fund Committee of China (Grant No. 11632014, 51808444), Scientific Research Program of Shanxi Provincial Education Department (18JK0502), State Key Laboratory for Strength and Vibration of Mechanical Structure open Foundation (Grant No. SV2018-KF-35), Startup Foundation of XUST (Grant No. 2018YQ2-05).

Institutional Review Board Statement: Not applicable.

Informed Consent Statement: Not applicable.

Data Availability Statement: The models and some data of the two typical circular tubular Vierendeel truss arches (the pin-ended and end-fixed) used in this study are available in the repository of GitHub via https://github.com/yunfeng-a/ABAQUS.git (accessed on 14 April 2023).

Conflicts of Interest: The authors declare no conflict of interest.

Appendix A

Table A1. Equations and their assumptions.

Equation (3)	$K_V = \dfrac{1}{\dfrac{L_c^2}{48EI_c} + \dfrac{L_cB}{24EI_t} + \dfrac{nL_c}{2BA_tG}}$	Sectional shear stiffness considering δ
Equation (4)	$GJ = G\dfrac{4A_0^2}{\sum\limits_{i=1}^{4}\frac{l_i}{t_{ri}}}$	Sectional torsional stiffness ignoring δ and GI_{pc}
Equation (8)	$GJ = \dfrac{H^2}{\dfrac{L_c^2}{12EI_c} + \dfrac{L_cB}{6EI_t} + \dfrac{2nL_c}{BA_tG}} + \dfrac{B^2}{\dfrac{L_c^2}{12EI_c} + \dfrac{L_cH}{6EI_t} + \dfrac{2nL_c}{HA_tG}}$	Sectional torsional stiffness considering δ
Equation (12)	$GJ = \dfrac{H^2}{\dfrac{L_c^2}{12EI_c} + \dfrac{L_cB}{6EI_t} + \dfrac{2nL_c}{BA_tG}} + \dfrac{B^2}{\dfrac{L_c^2}{12EI_c} + \dfrac{L_cH}{6EI_t} + \dfrac{2nL_c}{HA_tG}} + 4GI_{pc}$	Sectional torsional stiffness considering δ and GI_{pc}
Equation (13)	$q_{cr} = \dfrac{q_{cr0}}{1 + q_{cr0}R/K_V}$	Dou's equation of critical buckling load for pin-ended arches
Equation (14)	$q_{cr0} = \dfrac{P_y\left[1 - (\Theta/\pi)^2\right]^2}{R\left[1 + (EI_y/GJ)(\Theta/\pi)^2\right]}$	Kirchhoff's equation of critical buckling load for pin-ended arches
Equation (16)	$\begin{cases} q_{cr} = \dfrac{q_{cr0}}{1 + q_{cr0}R/K_V} \\ q_{cr0} = \dfrac{4\pi^2EI_y}{S^2R}\left[A\left(\dfrac{\Theta}{\pi}\right)^2 + B\left(\dfrac{\Theta}{\pi}\right) + 0.85\right] \end{cases}$	Numerically fitted equation of critical buckling load for end-fixed arches

References

1. Tianfu Agricultural Expo Main Hall—The Institution of Structural Engineers. Available online: http://www.istructe.org/structural-awards/projects/2022/tianfu-agricultural-expo-main-hall/ (accessed on 15 April 2023).
2. Chen, S. Analysis of longitudinally symmetrical vierendeel girders by the theorem of three shears. *J. ICE* **1948**, *30*, 192–194. [CrossRef]
3. Shehata, A.A.; Korol, R.M.; Mirza, F.A. Joint Flexibility Effects on Rectangular Hollow Section Vierendeel Trusses. *Mech. Based Des. Struct. Mach.* **1987**, *15*, 89–107. [CrossRef]
4. Pi, Y.-L.; Trahair, N.S. In-Plane Buckling and Design of Steel Arches. *J. Struct. Eng.* **1999**, *125*, 1291–1298. [CrossRef]
5. Pi, Y.-L.; Trahair, N.S. In-Plane Inelastic Buckling and Strengths of Steel Arches. *J. Struct. Eng.* **1996**, *122*, 734–747. [CrossRef]
6. Pi, Y.-L.; Bradford, M.A. In-plane strength and design of fixed steel I-section arches. *Eng. Struct.* **2004**, *26*, 291–301. [CrossRef]
7. Pi, Y.L.; Bradford, M.A.; Uy, B. In-plane stability of arches. *Int. J. Solids Struct.* **2002**, *39*, 105–125. [CrossRef]

8. Guo, Y.-L.; Yuan, X.; Bradford, M.A.; Pi, Y.-L.; Chen, H. Strength design of pin-ended circular steel arches with welded hollow section accounting for web local buckling. *Thin. Wall. Struct.* **2017**, *115*, 100–109. [CrossRef]
9. Chu, C.; Tong, G. Elastic-plastic stability of shear-deformable circular arches. *J. Constr. Steel Res.* **2021**, *182*, 106694. [CrossRef]
10. Guo, Y.-L.; Chen, H.; Pi, Y.-L. In-plane failure mechanisms and strength design of circular steel planar tubular Vierendeel truss arches. *Eng. Struct.* **2017**, *151*, 488–502. [CrossRef]
11. He, H.; Yuan, B.; Chen, H.; Wei, Y. In-plane failure mechanism and stability bearing capacity design of planar plate-tube-connected circular steel arches. *Mech. Based Des. Struct. Mach.* **2022**, *50*, 154–169. [CrossRef]
12. Zhu, B.-L.; Liu, W.-C.; Guo, Y.-L.; Wang, J.-X. In-plane stability behaviours and design of web-opened steel arch. *J. Constr. Steel. Res.* **2022**, *194*, 107326. [CrossRef]
13. Zhu, B.; Zhao, J.; Yang, Y. Design Method of Core-Separated Assembled Buckling Restrained Braces Confined by Two Lightweight Concrete-Infilled Tubes. *Appl. Sci.* **2023**, *13*, 4306. [CrossRef]
14. Shi, M.; Yuan, B.; Jiang, T.; Wei, Y. In-plane failure mechanisms and strength design of circular steel tubular Vierendeel truss arches with rectangular section. *Structures* **2021**, *29*, 1779–1790. [CrossRef]
15. Sakimoto, T.; Namita, Y. Out-of-plane buckling of solid rib arches braced with transverse bars. *Proc. JSCE* **1971**, *1971*, 109–116. [CrossRef] [PubMed]
16. Sakimoto, T.; Komatsu, S. Ultimate Strength Formula for Steel Arches. *J. Struct. Eng.* **1983**, *109*, 613–627. [CrossRef]
17. Guo, Y.-L.; Zhao, S.-Y.; Dou, C.; Pi, Y.-L. Out-of-plane strength design of spatially trussed arches with a rectangular lattice section. *J. Constr. Steel Res.* **2013**, *88*, 321–329. [CrossRef]
18. Pi, Y.; Bradford, M.A.; Trahair, N.; Chen, Y.Y. A further study offlexural–torsional buckling of elastic arches. *Int. J. Struct. Stab. Dyn.* **2005**, *05*, 163–183. [CrossRef]
19. Timoshenko, S.; Gere, J. *Theory of Elastic Stability*, 2nd ed.; McGraw-Hill: New York, NY, USA, 1961.
20. Papangelis John, P.; Trahair Nicholas, S. Flexural-Torsional Buckling of Arches. *J. Struct. Eng.* **1986**, *112*, 2494–2511. [CrossRef]
21. Yang, Y.B.; Kuo, S.R. Effect of Curvature on Stability of Curved Beams. *J. Struct. Eng.* **1987**, *113*, 1185–1202. [CrossRef]
22. Rajasekaran, S.; Padmanabhan, S. Equations of Curved Beams. *J. Eng. Mech.* **1989**, *115*, 1094–1111. [CrossRef]
23. Pi, Y.-L.; Bradford, M.A. Elastic flexural–torsional buckling of fixed arches. *Q. J. Mech. Appl. Math.* **2004**, *57*, 551–569. [CrossRef]
24. Bradford, M.A.; Pi, Y.L. Flexural–torsional buckling of fixed steel arches under uniform bending. *J. Constr. Steel Res.* **2006**, *62*, 20–26. [CrossRef]
25. Dou, C.; Guo, Y.-L.; Pi, Y.-L.; Zhao, S.-Y.; Bradford, M.A. Effects of shape functions on flexural–torsional buckling of fixed circular arches. *Eng. Struct.* **2014**, *59*, 238–247. [CrossRef]
26. Pi, Y.-L.; Bradford Mark, A. Out-of-Plane Strength Design of Fixed Steel I-Section Arches. *J. Struct. Eng.* **2005**, *131*, 560–568. [CrossRef]
27. Guo, Y.-L.; Zhao, S.-Y.; Pi, Y.-L.; Bradford, M.A.; Dou, C. An experimental study on out-of-plane inelastic buckling strength of fixed steel arches. *Eng. Struct.* **2015**, *98*, 118–127. [CrossRef]
28. Dou, C.; Pi, Y.-L. Flexural-Torsional Buckling Resistance Design of Circular Arches with Elastic End Restraints. *J. Struct. Eng.* **2016**, *142*, 04015104. [CrossRef]
29. Dou, C.; Guo, Y.-L.; Zhao, S.-Y.; Pi, Y.-L.; Bradford, M.A. Elastic out-of-plane buckling load of circular steel tubular truss arches incorporating shearing effects. *Eng. Struct.* **2013**, *52*, 697–706. [CrossRef]
30. Wang, S.; Liu, X.; Yuan, B.; Shi, M.; Wei, Y. Out-of-plane elastic buckling load and strength design of space truss arch with a rectangular section. *Front. Struct. Civ. Eng.* **2022**, *16*, 1141–1152. [CrossRef]
31. *ABAQUS, Version 6.14 Documentaion*; Dassault Systèmes Simulia Corp.: Providence, RI, USA, 2016.
32. Bradford, M.A.; Pi, Y.-L. A new analytical solution for lateral-torsional buckling of arches under axial uniform compression. *Eng. Struct.* **2012**, *41*, 14–23. [CrossRef]
33. Guo, Z.-T. *Bending and Torsion of Thin-Walled Rods*; China Science and Technology of China Press: Beijing, China, 1989.
34. *GB50017. 2017*; Code for Design of Steel Structures. Ministry of Construction of the People's Republic of China: Beijing, China, 2017.
35. Pi, Y.-L.; Trahair, N.S. Inelastic lateral buckling strength and design of steel arches. *Eng. Struct.* **2000**, *22*, 993–1005. [CrossRef]
36. *Eurocode3: Design of Steel Structures-Part 2: Steel Bridge*; European Committee for Standardization: Brussels, Belgium, 2003.
37. La Poutré, D.B.; Spoorenberg, R.C.; Snijder, H.H.; Hoenderkamp, J.C.D. Out-of-plane stability of roller bent steel arches—An experimental investigation. *J. Constr. Steel Res.* **2013**, *81*, 20–34. [CrossRef]
38. Dou, C.; Guo, Y.-L.; Zhao, S.-Y.; Pi, Y.-L. Experimental Investigation into Flexural-Torsional Ultimate Resistance of Steel Circular Arches. *J. Struct. Eng.* **2015**, *141*, 04015006. [CrossRef]
39. Chau, N.L.; Dao, T.-P.; Nguyen, V.T.T. An Efficient Hybrid Approach of Finite Element Method, Artificial Neural Network-Based Multiobjective Genetic Algorithm for Computational Optimization of a Linear Compliant Mechanism of Nanoindentation Tester. *Math. Probl. Eng.* **2018**, *2018*, 7070868. [CrossRef]
40. Nguyen, T.V.T.; Huynh, N.-T.; Vu, N.-C.; Kieu, V.N.D.; Huang, S.-C. Optimizing compliant gripper mechanism design by employing an effective bi-algorithm: Fuzzy logic and ANFIS. *Microsyst. Technol.* **2021**, *27*, 3389–3412. [CrossRef]